

The late Paleozoic paired metamorphic belt of southern Central Chile: Consequence of a near-trench thermal anomaly?

Guido M. Gianni^{1*}

¹ Consejo Nacional de Investigaciones Científicas y Técnicas (CONICET). Instituto Geofísico Sismológico Ing. Fernando Volponi (IGSV), Universidad Nacional de San Juan. San Juan, Argentina. Email: guidogianni22@gmail.com

Abstract

The hypothesis of a subduction-related Miyashiro-type paired metamorphic belt for the origin of the late Paleozoic igneous and metamorphic complex in the Andean Coastal Cordillera has remained unquestioned since its proposal in the early seventies. A synthesis of the advances in the study of these metamorphic rocks between 33°S and 42°S, revising field relations among geological units, and geochemical and geochronological data from the contemporaneous granitoids of the Coastal Batholith, highlights inconsistencies in this model. The record of short-lived forearc magmatism in the late Paleozoic intruding the partially synchronous accretionary prism, and geochemical and isotopic data from the igneous rocks indicating sources from the accretionary prism sediments and the back-top lithosphere, suggest a departure from typical subduction settings. I conclude that the anomalous configuration of the paired metamorphic belt and the associated Coastal Batholith resulted from a complex geodynamic process involving a near-trench thermal anomaly caused by the subduction of a trench-parallel mid-ocean ridge.

Keywords: Paired metamorphic belts; accretionary prism; Coastal Cordillera; mid-ocean ridge subduction.

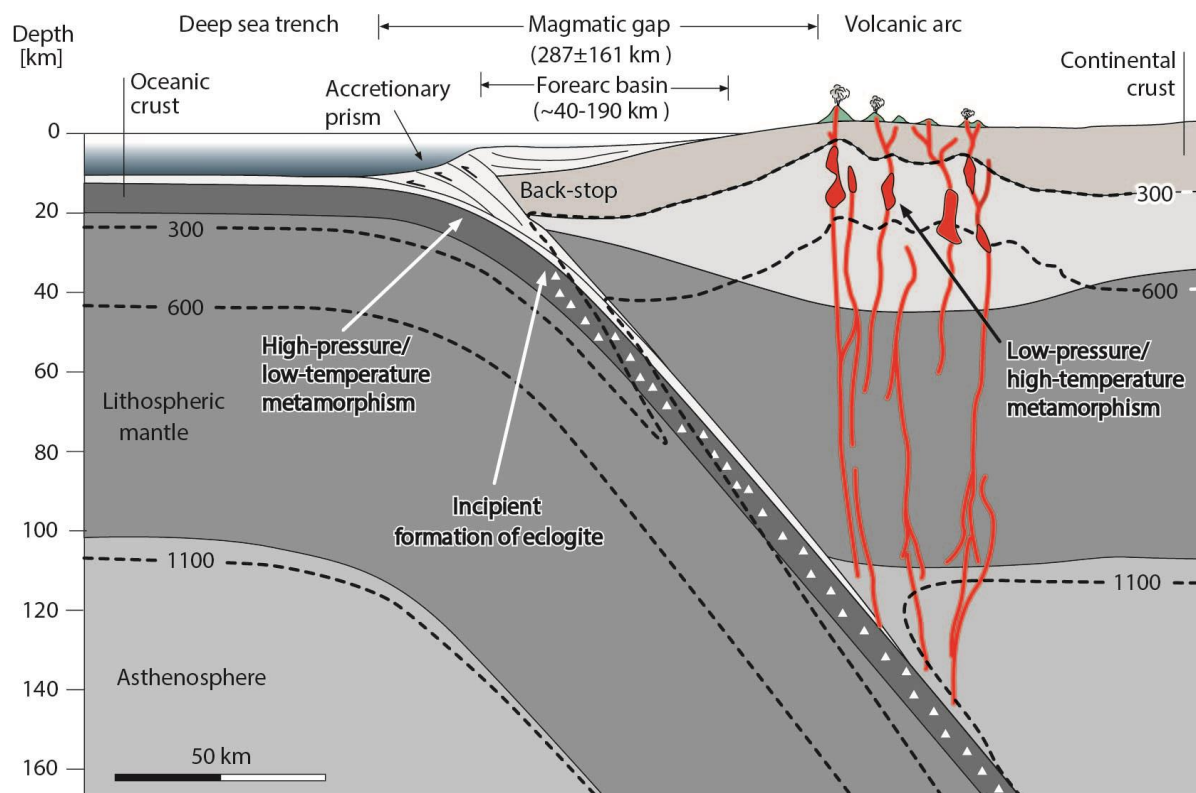
This is a non-peer reviewed preprint submitted to EarthArXiv

1. Introduction

The spatial arrangement of contemporaneous high-pressure/low-temperature metamorphic rocks and igneous intrusion-related low-pressure/high-temperature metamorphic rocks in Japan led Miyashiro to the novel idea that metamorphic belts could develop as a pair (Miyashiro, 1961).

28 Consolidation of the plate tectonic theory in the late 1960s provided a coherent framework for this
 29 idea, where paired metamorphic belts were explained as a direct result of the subduction process
 30 (Oxburgh and Turcotte, 1970; Ernst, 1971; Miyashiro, 1972; 1973). This was quantitatively
 31 demonstrated by the modeling of Oxburgh and Turcotte (1971), which showed that the oceanic
 32 plate subduction depresses the geotherm near the trench generating low-temperature/high-pressure
 33 metamorphism, which is preserved in the accretionary prism, and elevates the geotherm in the arc
 34 region causing high-temperature/low-pressure metamorphism (Fig. 1). Most recent studies have
 35 expanded this concept to collisional margins and included additional causes in subduction settings
 36 such as mid-ocean ridge-trench interactions and tectonic juxtaposition of laterally contemporaneous
 37 metamorphic belts (e.g., Brown, 1998a;b; 2009; 2010; Iwamori, 2000; Maruyama *et al.*, 2010).

38 Early studies in southern Central Chile highlighted similarities between the metamorphic
 39 zoning of late Paleozoic rocks in the Andean Coastal Cordillera and those described in Japan by
 40 Miyashiro (1961). In that region, a parallel and coeval arrangement of contrasting geological units
 41 was interpreted as a subduction-related high-pressure/low-temperature metamorphism to the west
 42 and a volcanic arc-related low-pressure/high-temperature metamorphism to the east that developed
 43 along the southwestern Gondwana margin (González-Bonorino and Aguirre, 1970; González-
 44 Bonorino, 1971; Aguirre *et al.*, 1972). In the last fifty years, numerous studies have supported the
 45 Pacific-type subduction hypothesis for the origin of the paired metamorphic belt in the Coastal
 46 Cordillera (Hervé *et al.*, 1974; 1984; 2013; Hervé, 1988; Kato and Godoy 1995; Duhart *et al.*, 2001;
 47 Glodny *et al.* 2005; 2008; Willner, 2005; Willner *et al.* 2005; Richter *et al.* 2007; Hyppolito *et al.*,
 48 2014a,b; 2015; Sigoña, 2016; Muñoz-Montecinos *et al.*, 2020).



49 *Figure 1. Cross-section through an active continental margin (modified from Frisch et al. 2010)*
50 *showing the approximate thermal structure in normal subduction settings, main areas of the*
51 *subduction system, and zones with contrasting metamorphism (Schubert and Turcotte, 1975).*
52 *The average arc-trench gap is from the Earthbyte group's website*
53 [\(https://www.earthbyte.org/calculating-arc-trench-distances-using-the-smithsonian-global](https://www.earthbyte.org/calculating-arc-trench-distances-using-the-smithsonian-global-volcanism-project-database/)
54 [volcanism-project-database/](https://www.earthbyte.org/calculating-arc-trench-distances-using-the-smithsonian-global-volcanism-project-database/)) *and the forearc basin width range is from Noda (2016).*

56 In this contribution, I first provide a synthesis of the advances in the study of these
57 metamorphic rocks and the Coastal Batholith (Fig. 2). Then, I discuss key field-based observations,
58 along with geochemical and geochronological data from the contemporaneous granitoids, and
59 contrast these data with our current understanding of the anatomy and dynamics of subduction
60 zones. This analysis highlights major inconsistencies in the Pacific-type subduction hypothesis for
61 the origin of the paired metamorphic belt of the Coastal Cordillera and suggests a more complex
62 late Paleozoic geodynamic setting than previously acknowledged.

63

64 **2. Paired metamorphic belt of the Coastal Cordillera in southern Central Chile**

65 Subduction complexes of Late Paleozoic and Mesozoic ages form a lengthy chain of >2000 km
66 extending from 32°-54°S that developed along the southwestern margin of Gondwana (Hervé,
67 1988). This revision deals with the basement rocks in the Coastal Cordillera of South Central Chile,
68 which extends between 32°S and 42°S, and is mostly concentrated on metasedimentary and igneous
69 units north of the Lanalhue fault zone (~39°S), where these form a contemporaneous paired
70 metamorphic belt (Fig. 2a). This area holds well-preserved outcrops of a late Carboniferous-Early
71 Permian metamorphic complex to the west and a contemporaneous batholith to the east jointly
72 interpreted as recording early subduction stages beneath southwest Gondwana (González-Bonorino
73 1970, 1971; González-Bonorino y Aguirre 1970; Aguirre *et al.* 1972; Hervé 1977; 1988; Hervé *et*
74 *al.* 1974; 1984; 2003; 2013; Mpodozis and Ramos; 1989; Beck *et al.*, 1991; Martin *et al.*, 1991;
75 Kato and Godoy 1995; Duhart *et al.*, 2001; Willner 2005; Willner *et al.* 2004; 2005; 2008; Glodny
76 *et al.* 2005; 2006; 2008) (Fig. 2a,b). In the following subsections, I summarize the main
77 characteristics of this igneous-metamorphic belt. In this synthesis, I focus on the most general
78 aspects of this belt, which are profound enough to highlight arguable aspects of the geodynamic
79 model proposed so far. In-depth details on metamorphic complexes and igneous rocks can be found
80 in the references provided in the text.

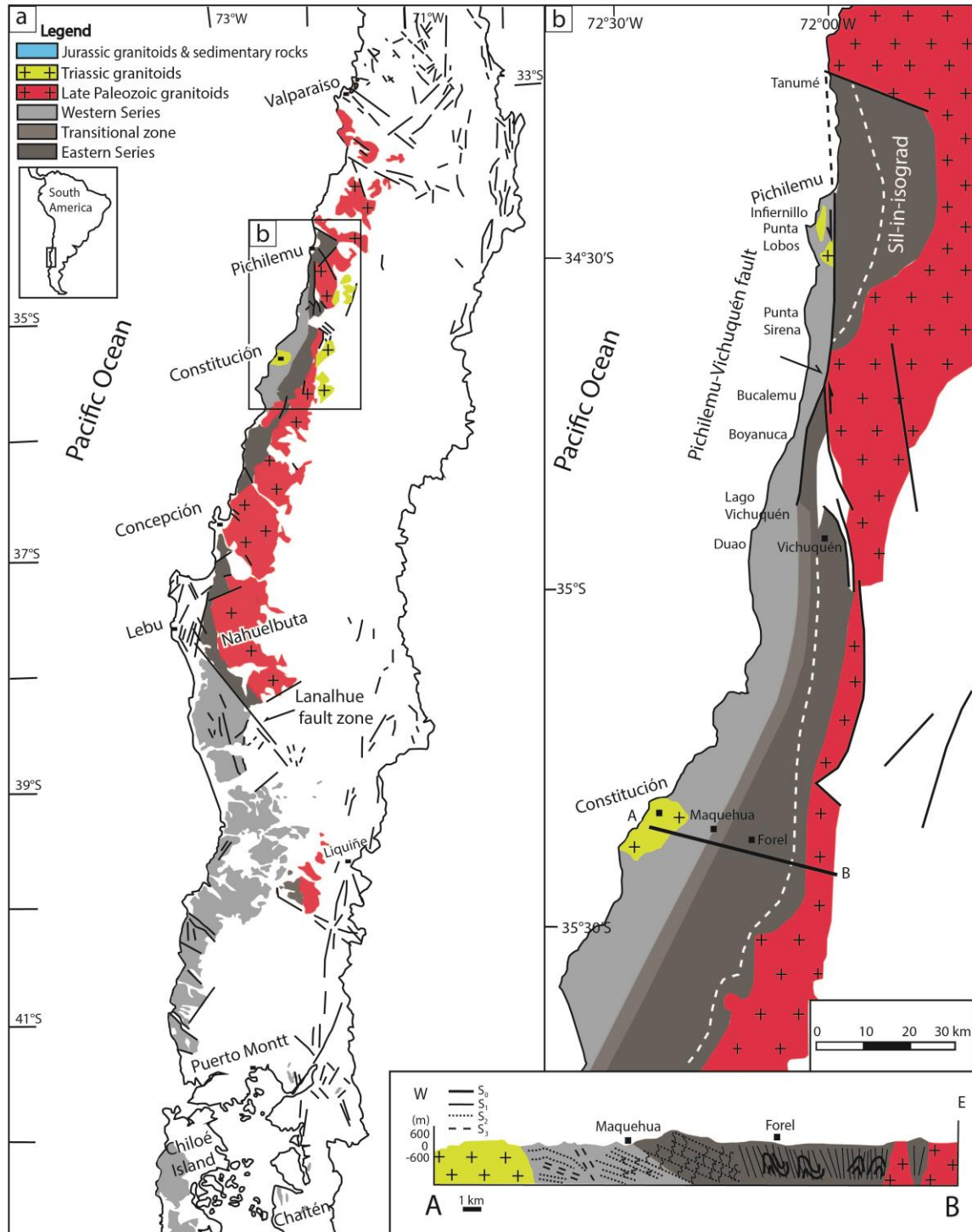
81

82 **2.1 Paired metamorphic belt of southern Central Chile**

83 The pioneering studies in the late Paleozoic basement rocks of Coastal Cordillera of southern
84 Central Chile by González-Bonorino and Aguirre (1970) and González-Bonorino (1971) identified
85 the Pichilemu, Curepto, and Nirivilo metamorphic facies series that depict a progressive appearance
86 of mineral zones and facies formed under diverse pressure, temperature, and tectonic regimes. The
87 metamorphic complex was later divided by Aguirre *et al.* (1972) into the Western and the Eastern
88 Series (Fig. 2a). The former are intensely deformed oceanic-derived high-pressure/low-temperature
89 units with sedimentary and basaltic protoliths of abyssal and trench environments, whereas the latter
90 is associated with less deformed trench-to-forearc metasedimentary rocks of very-low grade
91 overprinted by low-pressure/high-temperature metamorphism (González-Bonorino, 1971; Aguirre
92 *et al.*, 1972; Hervé *et al.*, 1984; Hervé, 1988; Willner, 2005; Hyppolito *et al.*, 2014a,b; 2015).

93 The late Paleozoic convergent stage that gave place to this accretionary complex was
94 preceded by a short-lived Devonian–early Carboniferous passive margin setting (~400–340 Ma,
95 Willner *et al.*, 2008, 2011 or 420–370 Ma, Hervé *et al.*, 2013) that changed to a convergent margin
96 with eastward polarity after ~340 Ma. Multi-method geochronological and structural studies
97 indicate that the accretionary prism would have grown from ~320 to ~224 Ma through frontal
98 accretion in the Eastern Series and basal accretion in the Western series with W and SW vergence
99 (Lohrmann, 2002; Glodny *et al.*, 2005; Willner *et al.*, 2005; Richter *et al.*, 2007) (Fig. 3). However,
100 Richter *et al.* (2007) suggested that the deepest portion of the Eastern Series was also affected by
101 basal accretion. Field-based analyses indicate that the nature of the contact between the Western
102 and Eastern Series is regionally variable, changing locally from transitional to tectonic (González-
103 Bonorino, 1971; Davidson *et al.*, 1987; Richter *et al.*, 2007; Willner *et al.*, 2009; Glodny *et al.*,
104 2008) (Fig. 2b). Maximum depositional ages obtained from detrital zircon dating in the
105 metasediments indicate early and late Carboniferous ages for the Eastern and Western series,
106 respectively, with provenance from older Gondwana margin basement of the Pampean (~530–510
107 Ma) and Famatinian (~470 Ma) belts, including reworked cratonic material, and Carboniferous
108 magmatism east of the present-day Andes (Duhart *et al.*, 2001; Willner *et al.*, 2008; Hervé *et al.*,
109 2013). However, south of the Lanalhue fault zone a Permian maximum depositional age has been
110 documented in the Western Series with detritus derived from the Choiyoi province (~287–245 Ma)
111 or subvolcanic plutonic rocks in the North Patagonian massif (~290–260 Ma) (Hervé *et al.*, 2013).
112 The Western Series is formed by schists and phyllites that contain meter- to kilometer-sized slices
113 of metabasites of high-pressure greenschists, epidote and garnet amphibolites, and blueschists
114 (Kato, 1985; Hervé, 1988; Shira *et al.*, 1990; Kato and Godoy 1995; Willner *et al.* 2004; Willner

115 2005; Hyppolito *et al.*, 2014a). The latter (~9.5–11 kbar, and 350–385°C) are scarce and the record
 116 of high-pressure conditions is given by greenschists that bear Na–



117
 118 *Figure 2. a) Geological sketch map of the studied area (34–42°S) showing the late Paleozoic*
 119 *metamorphic complexes and late Paleozoic and Triassic granitoids from the Coastal Batholith.*

120 *Figure modified from Hervé et al. (2013). b) Geological map of the Coastal Cordillera at Pichilemu*
121 *and Constitución regions (34°-35°40'S) with cross section A-B. Figure modified from Willner et al.*
122 *(2009).*

123 Ca amphibole and phengite (~7–9.3 kbar, and 380–420°C) and indicate a subduction-related
124 metamorphic gradient in the range of ~11–16 °C/km (Willner, 2005). Local occurrences of garnet-
125 bearing mica schists in the Punta Sirena region record the highest temperature conditions
126 (retrograde conditions in the range 9.6–14.7 kbar and 390–440°C, at ~320 Ma) and a counter-
127 clockwise P–T path (Willner, 2005) (Fig. 2b). Zircon dating of accreted sediments and ⁴⁰Ar–³⁹Ar
128 cooling ages in phengite from high-pressure greenschists from the Western Series indicates that
129 basal accretion began at ~308 Ma (Willner *et al.*, 2005, 2008; 2009, 2012; Hyppolito *et al.*, 2014b)
130 (Fig. 3). As demonstrated by Hyppolito *et al.* (2015), basal accretion preceded both the peak of
131 blueschist metamorphism at ~300 Ma in the Pichilemu region (Willner *et al.*, 2005) and cooling of
132 the Eastern Series in the interval 301–292 Ma (Fig. 3). During the evolution of the accretionary
133 complex, these rocks reached depths of 10–50 km and were later exhumed at variable rates ranging
134 from 0.03–2.0 mm/year (Willner *et al.*, 2004; Willner, 2005; Willner *et al.*, 2005; Kato *et al.*, 2008;
135 Hyppolito *et al.*, 2014b). Geochemical and isotopic studies indicate that metabasites from the
136 Western Series are ocean-derived tholeiitic and alkali basalts, with N-MORB, E-MORB, and OIB
137 signatures (Kato, 1985; Hervé, 1988; Kato & Godoy, 1995; Schira *et al.*, 1990; Hyppolito *et al.*,
138 2014a). These metabasites are interpreted as formed in an oceanic basin setting characterized by
139 shallow and deep mantle sources, such as plume-influenced mid-ocean ridge (Hyppolito *et al.*,
140 2014a).

141 The Eastern Series is formed by psammo-pelitic sequences associated with early
142 Carboniferous trench and Devonian passive margin sedimentary deposits that preserve bedding and
143 sedimentary structures (e.g., Hervé, 1988; Willner, 2005; Glodny *et al.*, 2008). The Eastern Series is
144 classically understood as the rear part of the late Paleozoic accretionary wedge, reflecting a position
145 transitional to the backstop area (Hervé, 1988; Willner *et al.*, 2000; Glodny *et al.*, 2008) (Fig. 4).
146 During the development of the accretionary wedge, the Eastern Series was intruded by late
147 Paleozoic granitoids belonging to the Coastal Batholith causing a metamorphic overprinting at 3
148 kbar (296–301 Ma, ⁴⁰Ar/³⁹Ar muscovite plateau ages, Willner *et al.*, 2005) of the very low-grade
149 frontal accretion-related metamorphism (Willner *et al.*, 2005; Glodny *et al.*, 2008; Hervé *et al.*,
150 2013; Deckart *et al.*, 2014) (Fig. 2a,b). Metamorphism in the Eastern Series records increasing
151 metamorphic grade from west to east, from greenschist to amphibolite and locally granulite facies
152 conditions and thermobarometric studies indicate high-temperature/low-pressure metamorphic
153 conditions in the range of 720–400°C and 2.5–3.5 kbar (Aguirre *et al.* 1972; Hervé, 1977; Willner

154 2005; Willner et al., 2005; Hyppolito et al., 2015). According to Hyppolito *et al.* (2015), the thermal
155 overprint occurred after the frontal accretion-related deformation (D1) and likely before or early
156 during the development of a penetrative foliation (S2) (Fig. 3). A contemporaneous paired
157 metamorphic belt in southern Central Chile has been corroborated by the age range for the high-
158 temperature metamorphism in the Eastern Series that falls into the time span determined for the
159 peak of high-pressure metamorphism in the Western Series at 292–320 Ma (Willner *et al.* 2005;
160 Hyppolito *et al.*, 2015) (Fig. 3).

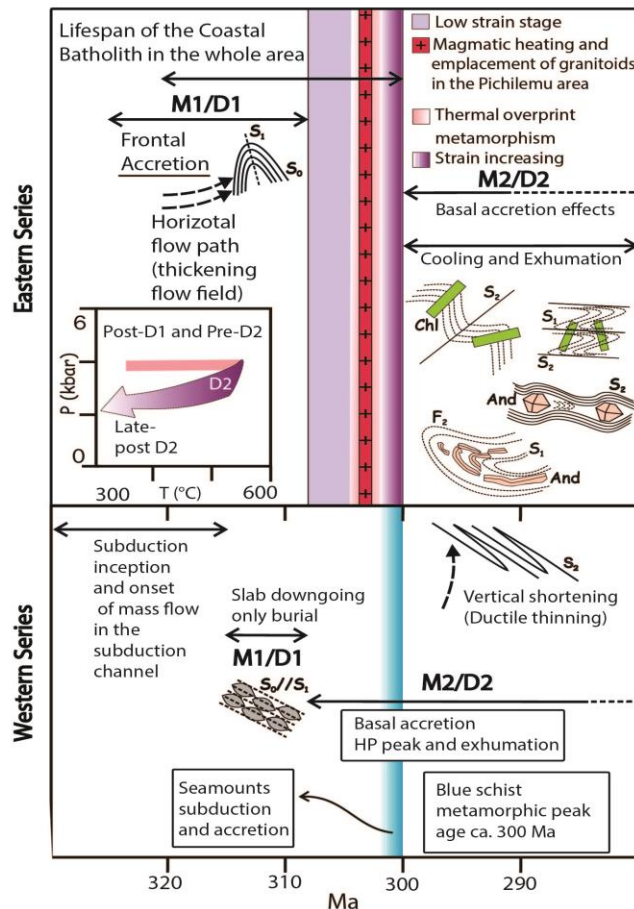
161

162 **3.2 The Coastal Batholith of southern Central Chile**

163 The Coastal Batholith crops out between 33°S and 38°20'S along the Coastal Cordillera and
164 is dislocated to the east by the Lanalhue strike-slip fault at 40°S (Glodney *et al.*, 2008) (Fig. 2a).
165 This is a large composite calc-alkaline igneous body of meta- to peraluminous composition mostly
166 made of tonalite, granodiorites, and granite with minor diorite that intruded syn- and post-
167 tectonically metamorphic rocks of the Eastern series (Cordani *et al.*, 1976; Hervé *et al.*, 1988; 2013;
168 Parada, 1999; Parada *et al.*, 1999; 2007; Charrier *et al.*, 2015). More locally, equivalent mafic rocks
169 have also been described intruding in basally accreted rocks of the Choapa Metamorphic Complex
170 (~318 Ma, Sigoña, 2016). Radiometric ages obtained in previous studies along the length of the
171 batholith yielded Late Carboniferous (Pennsylvanian) ages, mostly between ~300 and 320 Ma,
172 indicating a short-lived magmatic event (K-Ar, Cordani *et al.*, 1976; Rb-Sr isochron ages, Shibata *et al.*,
173 1984; U-Pb zircon ages, Godoy and Loske, 1988; Rb-Sr isochron and K-Ar ages, Hervé *et al.*,
174 1988; K/Ar and $^{40}\text{Ar}/^{39}\text{Ar}$, Beck *et al.*, 1991, K-Ar ages, Martin *et al.* 1991; U-Pb zircon ages, Gana
175 and Tosdal, 1996; Rb-Sr isochron, Lucassen *et al.*, 2004; two-point Rb-Sr ages, Glodny *et al.*, 2008;
176 U-Pb zircon ages, Pineda and Calderón, 2008; U-Pb SHRIMP zircon ages, Deckart *et al.*, 2014).
177 As mentioned in the previous subsection, the intrusion of this large igneous body is responsible for
178 the metamorphic overprint at around 300 Ma on the eastern side of the Eastern Series (e.g., Willner
179 *et al.*, 2005; Hyppolito *et al.*, 2015) (Figs. 2b and 3). Also, ages for the metamorphic peaks on the
180 basally accreted Western Series indicate that metamorphism overlapped with the intrusion of the
181 Coastal Batholith (Willner et al., 2005; Hervé *et al.* 2013) (Fig. 3).

182 Based on the analysis of Carboniferous mafic enclaves Parada *et al.* (1999) noted that in
183 terms of Y, La, and Nb, these have geochemical signatures of continental basalts derived from an
184 enriched lithospheric mantle. These authors indicated that the Sr–Nd isotope data (Initial $^{87}\text{Sr}/^{86}\text{Sr}$ =
185 0.7057 - 0.7098 and ϵNd = -2 - -4) suggest that these mafic rocks were derived from primary
186 enriched mantle-derived magmas. Lucassen *et al.* (2004) also found enriched isotopic compositions
187 in the late Paleozoic Nahuelbuta granitoids presenting initial $^{87}\text{Sr}/^{86}\text{Sr}$ ratios between 0.705 and

188 0.715 and ϵNd values between -2.5 and -7.5 (Fig. 2a). These authors noted that the REE patterns in
 189 late Paleozoic rocks of the Coastal Batholith are similar to those of the metamorphic accretionary
 190 basement and an average upper continental crust that together, with their isotopic composition,
 191 indicate a crustal origin. Recently, Deckart *et al.* (2014) showed that Lu-Hf isotopic analyses on
 192 zircon grains with ages between ~320 and 300 Ma have initial $\epsilon\text{Hf}(i)$ values from +1.67 - -5.64,
 193 with most of the analyses between +1 and -4 epsilon units and the T_{DM2} in these rocks suggest
 194 Mesoproterozoic crustal residence ages. These authors also presented $\delta_{18}\text{O}$ ratios from the dated
 195 zircon grains ranging from 6.4 - 8.6‰ with a prominent group with values between 6.0 and 7.5‰
 196 and a minor group between 8.0 and 9.0‰. According to Deckart *et al.* (2014), these data indicate
 197 that the magmas were likely derived from crustal sources with a prominent sedimentary input as
 198 suggested by the elevated $\delta_{18}\text{O}$ values. However, as pointed out by these authors, a mantle input
 199 cannot be completely ruled out. Therefore, geochemical and isotopic data suggest that the Coastal
 200 Batholith has a high proportion of reworked old crustal material, indicating that either the magmas
 201 assimilated large amounts of metasediments from Eastern Series, which represent reworked old
 202 continental crust, and/or that the Eastern Series was partly underlain by an old continental back-stop
 203 basement (Parada *et al.*, 1999; Lucassen *et al.*, 2004; Glodny *et al.*, 2006; Deckart *et al.*, 2014).



205 *Figure 3. Image depicting the temporal relations between deformation in Western and Eastern*
206 *series, and the overall evolution of the accretionary wedge in the Pichilemu region. Figure modified*
207 *from Hyppolito et al. (2015). See text for discussion.*

208

209 The geodynamic context of the Coastal Batholith is classically interpreted as a subduction
210 setting where this igneous body represents part of the large southwestern Gondwana magmatic arc
211 (Hervé *et al.*, 1988; Parada, 1990; Parada *et al.*, 1999; 2007; Lucassen *et al.*, 2004; Charrier *et al.*,
212 2007; 2015; Deckart *et al.*, 2014; del Rey *et al.*, 2016; Oliveros *et al.*, 2020; among others).
213 According to the regional analysis of Charrier *et al.* (2015), differences in peak metamorphic ages
214 in accretionary complexes north of 33°S and the contrasting ages of igneous rocks south and north
215 of this latitude likely indicate a major segmentation in the ancient convergent margin.

216

217 **3. Discussion: A circum-Pacific Miyashiro-type or a forearc paired metamorphic belt in** 218 **south Central Chile?**

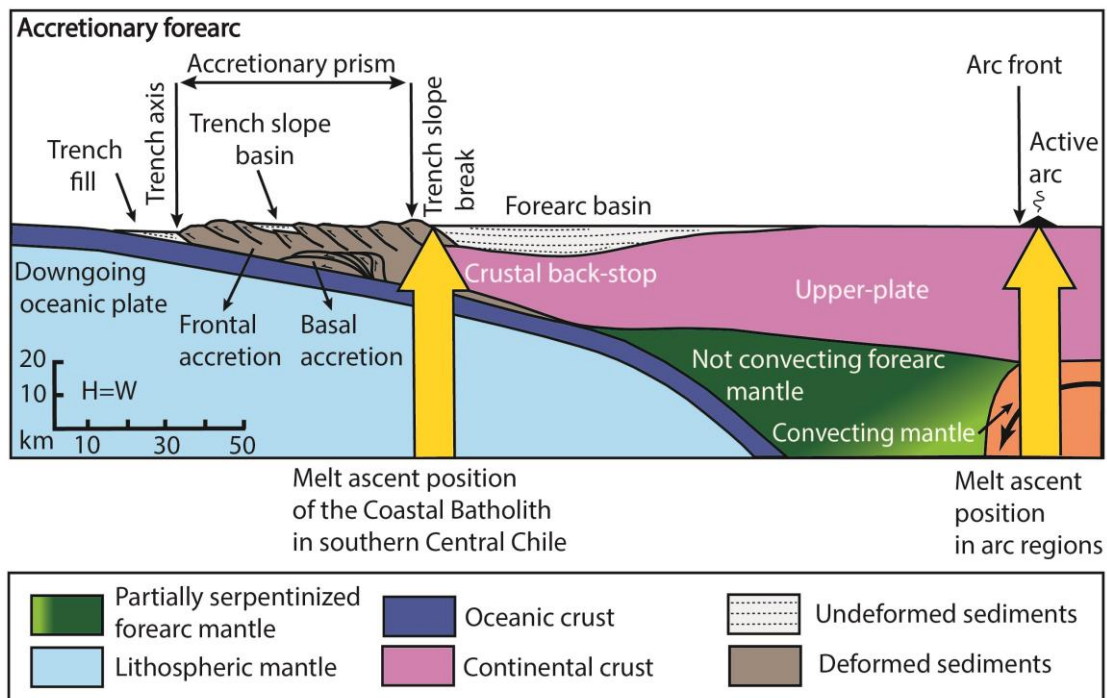
219 The hypothesis of a circum-Pacific Miyashiro-type paired metamorphic belt for the origin of the
220 late Paleozoic igneous-metamorphic complexes of south Central Chile has remained unquestioned
221 since its proposal in the seventies (González-Bonorino and Aguirre, 1970; González-Bonorino,
222 1971; Aguirre *et al.*, 1972; Hervé *et al.*, 1974, 1984, 2013; Hervé, 1988; Kato, 1985; Kato and
223 Godoy 1995; Duhart *et al.*, 2001; Glodny *et al.* 2005; 2008; Willner 2005; Willner *et al.* 2005;
224 Richter *et al.* 2007; Hyppolito *et al.*, 2014a,b; 2015; Muñoz-Montecinos *et al.*, 2020). Below I argue
225 that field relations between the metamorphic and igneous units, and possibly the time and
226 geochemistry of the Coastal Batholith, highlight inconsistencies in this model and are not
227 compatible with our current understanding of typical subduction zones.

228 The geological configuration of subduction zones indicates that the contemporaneous arc and
229 accretionary prism systems do not overlap and that both develop under contrasting geothermal
230 gradients, which constitute the foundations of Miyashiro's concept of paired metamorphic belts
231 (e.g., Oxburgh and Turcotte, 1971; Stern, 2002) (Fig. 1). Global analyses of active subduction
232 zones indicate that average arc-trench gaps are 287 ± 161 km ([https://www.earthbyte.org/calculating-
233 arc-trench-distances-using-the-smithsonian-global-volcanism-project-database/](https://www.earthbyte.org/calculating-arc-trench-distances-using-the-smithsonian-global-volcanism-project-database/)) and the rear areas
234 of accretionary prisms are commonly separated from arc regions by ~40-190 km wide forearc
235 basins (Noda, 2016) (Figs. 1 and 4). Notably, this distance could be larger if forearc fold-and-thrust
236 belts are present as recently recognized in some areas of the Andes (e.g., Armijo *et al.* 2015;
237 Riesner *et al.*, 2018; Martinez *et al.*, 2020; Encinas *et al.*, 2020). Volcanic arcs and accretionary

238 prisms do not superpose even in subduction settings with the highest known slab angles, such as
239 Mariana-type subduction zones with up to 90° dipping slabs (Uyeda and Kanamori, 1979). An
240 apparent superposition of these two systems is possible when subsequent tectonic processes, such as
241 strike-slip or forearc underthrusting, juxtapose the geological record of both areas (e.g., Brown *et*
242 *al.*, 1998a,b; 2010). In the case of the igneous-metamorphic complexes in the Coastal Cordillera
243 between 33°S and 42°S, a tectonic superposition of both belts is ruled out by field relations, and
244 despite subsequent deformation during Andean orogeny, an in-situ formation has been
245 demonstrated (e.g., Willner *et al.*, 2005). Detailed mapping in the last decades has confirmed early
246 observations on the intrusive nature of the contact between the Coastal Batholith and the Eastern
247 Series, and established a transitional contact between the latter and the Western Series at several
248 latitudes (González-Bonorino, 1971; Davidson *et al.*, 1987; Richter *et al.*, 2007; Willner *et al.*,
249 2009) (Fig. 2b). Also, Sigoña (2016) documented ~318 Ma mafic dykes associated with the Coastal
250 Batholith intruding high-pressure/low-temperature rocks at 31°30'S. The latter observations
251 constitute a challenge for the interpretation of a circum-Pacific-type paired metamorphic belt for
252 late Paleozoic rocks in this area. The fact that throughout the development of the accretionary
253 wedge, the frontally accreted Eastern Series was intruded by the partially contemporaneous Coastal
254 Batholith (~320-300 Ma) (Willner *et al.*, 2005; Hervé *et al.*, 2013, 2014; Deckart *et al.*, 2014),
255 indicate a geodynamic setting that departs substantially from typical subduction zones (Fig. 4). In
256 the latter, magmatic activity is usually concentrated several kilometers away from the accretionary
257 prisms and is developed above a mantle wedge (e.g., Stern, 2002; Tatsumi, 2005; Gerya and
258 Meilick, 2011) (Figs. 1 and 4). A major implication of the proximity of the igneous activity to the
259 paleo-trench is that the proposed magmatic arc nature of the Coastal Batholith is untenable (e.g.,
260 Hervé, 1988; Parada, 1990; Parada *et al.*, 1999; 2007; Lucassen *et al.*, 2004; Deckart *et al.*, 2014;
261 Sigoña, 2016). The abnormal character of the Coastal Batholith is not only limited to the
262 conspicuous emplacement site within the overall subduction system (Fig. 4). Deckart *et al.* (2014)
263 already highlighted that the short period of time of batholith emplacement (~20 Ma) and the
264 petrogenetic features indicating a major source from the accretionary prism metasediments and/or
265 the back-stop lithosphere (Parada, 1990; Parada *et al.*, 1999; Lucassen *et al.*, 2004) contrast those of
266 typical cordilleran batholiths. The latter, are commonly formed along tens or hundred million years
267 through multiple pulses of magmatism with variable mantle wedge and crust inputs depending,
268 among other parameters, on the upper-plate nature and thickness (e.g., Ducea *et al.*, 2015). Indeed,
269 these key observations have been integrated into evolutionary models of most recent studies at these
270 latitudes depicting a magmatic activity to the east that intrudes the frontally accreted Eastern series
271 and interacts with a potential back-stop lithosphere during magma ascent (e.g., Glodney *et al.*, 2008;

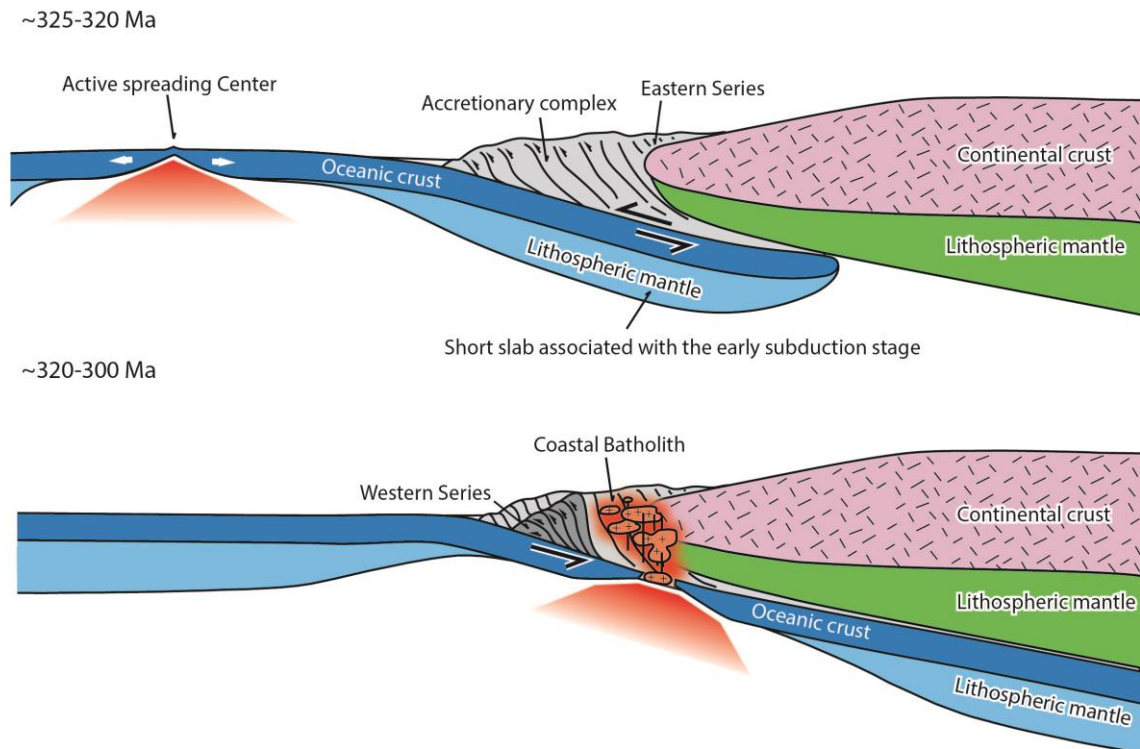
272 Hyppolito et al., 2014b; Díaz-Alvarado *et al.*, 2019). However, the geodynamic meaning of such an
 273 unusual geological configuration has been overlooked so far, and a continental arc setting was
 274 suggested in the latter and subsequent studies as well (e.g., del Rey *et al.*, 2016; Oliveros *et al.*,
 275 2020).

276 According to Willner *et al.* (2004; 2005), deep transport of a considerable volume of sediments
 277 below the upper mantle wedge during subduction initiation could have provided hydrous fluids
 278 triggering fluid-flux mantle melting and magmatism at the earliest stage in the evolution of the
 279 paired metamorphic belt. However, the latter cannot effectively explain the mainly crustal-like
 280 sources in the Coastal Batholith (Parada, 1990; Parada *et al.*, 1999; Lucassen *et al.*, 2004; Deckart
 281 *et al.*, 2014). Alternatively, Deckart *et al.* (2014) proposed that deeply subducted sediments could
 282 have been melted at mantle depths, which is compatible with isotopic values of the Coastal
 283 Batholith. Nevertheless, in either case, deep sediment subduction up to the mantle wedge within a
 284 shallow subduction setting, as inferred at the onset of convergence in this region (Willner *et al.*,
 285 2004), would have still triggered magmatism far from the accretionary prism. The latter is also
 286 confirmed by 2-D numerical modeling studies where buoyant plumes of partially melted sediments
 287 in the mantle wedge ascend several kilometers away from accretionary prisms impacting beneath
 288 the arc and backarc areas, even at normal slab angles (30-45°) (Gerya and Yuen, 2003; Gerya and
 289 Meilick, 2011)



291 *Figure 4. Cross-section in scale of an accretionary forearc (modified after Stern, 2002). This image*
292 *illustrates the unusual setting where the Coastal Batholith of southern Central Chile was emplaced*
293 *during the late Paleozoic.*

294 To trigger substantial magmatic activity in the overall cold forearc region, a thermal anomaly is
295 needed below the rear part of the late Paleozoic accretionary prism. Although not common in
296 normal subduction zones, forearc magmatism and related high-temperature/low-pressure
297 metamorphism have been documented in recent and ancient convergent settings in association with
298 asthenosphere upwelling produced by the development of slab gaps (e.g., Uyeda and Miyashiro,
299 1974; Marshak and Karig, 1977; DeLong and Fox, 1979; Iwamori, 2000; Wakabayashi, 2004;
300 Santosh and Kusky, 2010; see Gianni and Perez-Luján, 2021, for a recent synthesis). Slab windows
301 or gaps are openings in the downgoing plate that allow hot sub-slab asthenosphere to flow through
302 the slab hole impacting beneath the upper-plate margin. This phenomenon influences the arc and
303 backarc magmatism (e.g., Abratis, and Wörner, G., 2001; Rosenbaun *et al.*, 2008; Thorkelson *et al.*,
304 2011), the upper-plate thermal structure (Roche *et al.*, 2018; Ávila and Dávila, 2018), the mantle
305 flow in subduction zones, and the overall plate kinematics (Guillaume *et al.*, 2010; Király *et al.*,
306 2020). Slab gap development can be produced by several processes but mostly results from two
307 general causes. One is the presence of buoyancy anomalies in the downgoing plate such as oceanic
308 plateaus, aseismic ridges, or continental fragments (e.g., Cloos, 1993) that resist subduction and
309 lead to slab ruptures. The latter could be caused by local slab necking forming holes within the
310 downgoing plate (e.g., Király *et al.*, 2020), vertical slab tearing (e.g., Rosenbaun *et al.*, 2008), or by
311 the propagation of horizontal tears (e.g., Wortel and Spakman, 2000). The other cause of slab gap
312 development comprises the divergence or reactivation and separation of a preexisting plate
313 discontinuity such as the separation of an active spreading center during subduction (Uyeda and
314 Miyashiro, 1974; DeLong and Fox, 1979; Marshak and Karig, 1977; Dickinson and Snyder, 1979)
315 or a major fault onboard the oceanic plate such as fracture zones and transform faults (e.g., Pesicek
316 *et al.*, 2012). Although most of the processes forming slab gaps induce more or less similar
317 magmatic and thermal effects in the upper-plate, mid-ocean ridge subduction is characterized by a
318 substantial impact on the forearc area. In that region, ridge subduction may cause uplift and
319 unconformity development, local ophiolites emplacement, near-trench MORB (Mid-Ocean-Ridge-
320 Basalt) intrusions, felsic magmatism by crustal anatexis of the accretionary prism (*blow-torch*
321 *effect*, DeLong *et al.*, 1979), and low-pressure/high-temperature metamorphism (Marshak and
322 Karig, 1977; DeLong *et al.*, 1979; Nelson *et al.*, 1993; Underwood *et al.*, 1993; see Sisson *et al.*,
323 2003, for a synthesis). In this context, heating and melting of the accretionary prism can take place
324 with or without cessation of subduction (Underwood *et al.*, 1993;



325

326 *Figure 5. Conceptual model of a forearc paired metamorphic belt for the origin of the igneous-*
 327 *metamorphic complexes of the Coastal Cordillera of southern Central Chile (33°-40°S (modified*
 328 *from Wakabayashi, 2004).*

329

330 Brown, 1998b; Iwamori, 2000). Subduction of a trench-parallel mid-ocean ridge segment could be a
 331 possible explanation for the short-lived thermal anomaly (~20 Ma) beneath the rear part of the late
 332 Paleozoic accretionary prism and the formation of the Coastal Batholith (Fig. 5). According to the
 333 2-D numerical modeling of Iwamori (2000), initial mid-ocean ridge subduction can drive high-
 334 temperature/low-pressure metamorphism and magmatism before the opening of a slab window
 335 explaining near-trench granitoids coexisting with paired metamorphic belts. The latter study found
 336 that ridge crest subduction produces a substantial thermal anomaly that depending on plate
 337 kinematics can be dissipated in up to 30 Myr after the ridge subduction event. Hence, subduction of
 338 an active spreading center and possibly the incipient ridge opening during initial subduction could
 339 have provided the necessary heat and fluids to melt materials from the rear accretionary prism and
 340 back-stop lithosphere, which is compatible with the isotopic and geochemical signatures of the
 341 Coastal Batholith (Parada, 1990; Parada *et al.*, 1999; Lucassen *et al.*, 2004; Deckart *et al.*, 2014)
 342 (Fig. 5). Local occurrences of equivalent forearc magmatic activity along the coast at 28°30-

343 29°30'S described by Creixell *et al.* (2016) likely indicate that a similar process could have taken
344 place to the north of the study area. Therefore, the igneous-metamorphic rocks of the Coastal
345 Cordillera of southern Central Chile (33°-42°S) could have been formed as a forearc-type paired
346 metamorphic belt, whose spatio-temporal relations indicate an origin associated with a near-trench
347 thermal anomaly (Fig. 5). The short time spanned between the onset of subduction and the forearc
348 magmatism (~20 Myr), and the apparent lack of an arc region to the east, attesting for subduction
349 magnitudes below the critical slab dehydration depth (120 ± 40 km) necessary for fluid flux melting
350 in the mantle wedge (Tatsumi, 2005), indicate that the ridge would have been located relatively near
351 the Devonian passive margin of southwest Gondwana (Fig 5).

352

353 **4. Conclusion**

354 A revision of metamorphic rocks and the contemporaneous igneous intrusions along the coast
355 of southern Central Chile challenges the pioneering hypothesis of a subduction-related Miyashiro-
356 type paired metamorphic belt for the origin of this igneous-metamorphic complex. The short-lived
357 intrusion of the Coastal Batholith in the rear area of the partially synchronous accretionary wedge,
358 and geochemical and isotopic data from the igneous rocks indicating substantial participation of
359 sources from the accretionary prism and the back-top lithosphere, are not compatible with typical
360 subduction settings. I suggest that the igneous-metamorphic rocks from the study area formed as a
361 forearc-type paired metamorphic belt. The latter would have resulted from a near-trench thermal
362 anomaly triggered by the subduction of a mid-ocean ridge crest in late Paleozoic times.

363

364 **Acknowledgements**

365 G.M.G. recognizes the support received by CONICET and discussion with several members of the
366 Laboratorio de Tectónica Andina and the Instituto Sismológico Ing. Fernando Volponi (IGSV)
367 through the years.

368

369 **References**

370 Abratis, M., Wörner, G., 2001. Ridge collision, slab-window formation, and the flux of Pacific
371 asthenosphere into the Caribbean realm. *Geology*, 29(2), 127-130.

372 Armijo, R., Lacassin, R., Coudurier-Curveur, A., Carrizo, D., 2015. Coupled tectonic evolution of
373 Andean orogeny and global climate. *Earth-Science Reviews*, 143, 1-35.

374 Aguirre, L., Hervé, F., Godoy, E., 1972. Distribution of metamorphic facies in Chile, an outline.
375 *Kristalinikum*, Prague, 9, p. 7–19.

376 Ávila, P., Dávila, F. M., 2018. Heat flow and lithospheric thickness analysis in the Patagonian
377 asthenospheric windows, southern South America. *Tectonophysics*, 747, 99-107.

378 Beck, M.E. Jr., Garcia, R. A., Burmester, R.F., Munizaga, F., Hervé, F., Drake, R.E., 1991.
379 Paleomagnetism and geochronology of late Paleozoic granitic rocks from the Lake District of
380 southern Chile: implications for accretionary tectonics. *Geology*, 19, 332-335.

381 Brown, M., 1998a. Unpairing metamorphic belts: P–T paths and a tectonic model for the Ryoke
382 belt, southwest Japan. *Journal of Metamorphic Geology*, 16, 3–22.

383 Brown, M., 1998b. Ridge –trench interactions and high-T–low-P metamorphism, with particular
384 reference to the cretaceous evolution of the Japanese islands. In: Treloar, P.J., O’Brien, P.J. (Eds.),
385 *What Drives Metamorphism and Metamorphic Reactions?* Special Publication-Geological Society
386 of London, vol. 138, pp. 137 – 169.

387 Brown, M., 2009. Metamorphic patterns in orogenic systems and the geological record. In:
388 Cawood, P.A., Kröner, A. (Eds), *Accretionary Orogens in Space and Time*. Geological Society,
389 London, Special Publications vol. 318, pp. 37–74.

390 Brown, M., 2010. Paired metamorphic belts revisited. *Gondwana Research*, 18(1), 46-59.

391 Charrier, R., Pinto, L., Rodríguez, M. P., 2007. Tectonostratigraphic evolution of the Andean
392 Orogen in Chile. In: Moreno, T. & Gibbons, W. (eds) *The Geology of Chile*. Geological Society,
393 London, 21–114.

394 Charrier, R., Ramos, V. A., Tapia, F., Sagripanti, L., 2015. Tectono-stratigraphic evolution of the
395 Andean Orogen between 31 and 37 S (Chile and Western Argentina). *Geological Society, London*,
396 *Special Publications*, 399(1), 13-61.

397 Cloos, M., 1993. Lithospheric buoyancy and collisional orogenesis: Subduction of oceanic plateaus,
398 continental margins, island arcs, spreading ridges, and seamounts. *Geological Society of America*
399 *Bulletin*, 105(6), 715-737.

400 Cordani, U., Munizaga, F., Hervé, F., Hervé, M., 1976. Edades radiométricas provenientes del
401 basamento cristalino de la Cordillera de la Costa de las provincias de Valparaíso y Santiago, Chile.
402 In *Congreso Geológico Chileno*, No. 1, Actas 2: F213-F221. Santiago.

403 Creixell, C., Oliveros, V., Vásquez, P., Navarro, J., Vallejos, D., Valin, X., Godoy, E., Ducea,
404 M.N., 2016. Geodynamics of late carboniferous early Permian forearc in north Chile (28°30'-29°30'
405 S). *Journal of the Geological Society of London*, 173(5), 757–772.

406 Davidson, J., Mpodozis, C., Godoy, E., Hervé, F., Pankhurst, R., Brook, M., 1987. Late Paleozoic
407 accretionary complexes on the Gondwana margin of southern Chile: Evidence from the Chonos
408 Archipelago. *Gondwana Six: Structure, Tectonics, and Geophysics*, 40, 221-227.

409 Deckart, K., Hervé, F., Fanning, C.M., Ramírez, V., Calderón, M., Godoy, E., 2014. U-Pb
410 geochronology and Hf-O isotopes of zircons from the Pennsylvanian Coastal Batholith, South-
411 Central Chile. *Andean Geology*, 41, 49-82.

412 DeLong, S.E., Schwarz, W.M., Anderson, R.N., 1979. Thermal effects of
413 ridge subduction. *Earth Planetary Science Letters*, 44, 239–246.

414 Del Rey, A., Deckart, K., Arriagada, C., Martínez, F., 2016. Resolving the paradigm of the late
415 Paleozoic–Triassic Chilean magmatism: Isotopic approach. *Gondwana Research*, 37, 172-181.

416 Díaz-Alvarado, J., Galaz, G., Oliveros, V., Creixell, C., Calderón, M., 2019. Fragments of the
417 late Paleozoic accretionary complex in central and northern Chile: similarities and differences as a
418 key to decipher the complexity of the pre-Andean cycle. A. Folguera, B. Horton (Eds.), *Andean*
419 *Tectonics*, Elsevier.

420 Dickinson, W.R., and Snyder, W.S., 1979. Geometry of triple junctions related
421 to San Andreas transform. *Journal of Geophysical Research*, 84, 561–572.

422 Ducea, M. N., Saleeby, J. B., Bergantz, G., 2015. The architecture, chemistry, and evolution of
423 continental magmatic arcs. *Annual Review of Earth and Planetary Science Letters*, 43, 299-331.

424 Duhart, P., Mc Donough, M., Muñoz, J., Martin, M., Villeneuve, M., 2001. El Complejo
425 Metamórfico Bahía Mansa en la Cordillera de la Costa del centro-sur de Chile (39°30'–42°S):
426 geocronología K/Ar, ⁴⁰Ar/³⁹Ar y U/Pb, implicancias en la evolución del margen sur-occidental de
427 Gondwana. *Revista Geológica de Chile*, 28, 179–208.

428 Encinas, A., Sagripanti, L., Rodríguez, M. P., Orts, D., Anavalón, A., Giroux, P., Otero, J.,
429 Echaurren, A., Zambrano, P., Valencia, V., 2020. Tectonosedimentary evolution of the Coastal
430 Cordillera and Central Depression of south-Central Chile (36° 30'-42° S). *Earth-Science Reviews*,
431 103465.

432 Ernst, W.G., 1971. Metamorphic zonations on presumably subducted lithospheric plates from
433 Japan, California and the Alps. *Contributions to Mineralogy and Petrology*, 34, 43–59.

434 Frisch, W., Meschede, M., Blakey, R., 2011. Plate tectonics: continental drift and mountain
435 building. Springer-Verlag Berlin Heidelberg, pp. 149–158

436 Gana, P., Tosdal, R., 1996. Geocronología U-Pb y K-Ar en intrusivos del Paleozoico y Mesozoico
437 de la Cordillera de la Costa, Región de Valparaíso, Chile. *Revista Geológica de Chile*, 23 (2), 151-
438 164.

439 Gerya, T. V., Yuen, D. A., 2003. Rayleigh–Taylor instabilities from hydration and melting propel
440 ‘cold plumes’ at subduction zones. *Earth and Planetary Science Letters*, 212(1-2), 47-62.

441 Gerya, T. V., Meilick, F. I., 2011. Geodynamic regimes of subduction under an active margin:
442 effects of rheological weakening by fluids and melts. *Journal of Metamorphic Geology*, 29(1), 7-31.

443 Gianni, G. M., Luján, S. P., 2021. Geodynamic controls on magmatic arc migration and
444 quiescence. *Earth-Science Reviews*, 103676.

445 Gill, J. B., 1981. *Orogenic andesites and plate tectonics* Springer-Verlag. New York, 390.

446 Glodny, J., Lohrmann, J., Echtler, H., Gräfe, K., Seifert, W., Collao, S., Figueroa, O., 2005. Internal
447 dynamics of a paleoaccretionary wedge: insights from combined isotope tectonochronology and
448 sandbox modelling of the South-Central Chilean forearc. *Earth and Planetary Science*
449 *Letters*, 231(1-2), 23-39.

450 Glodny, J., Echtler, H. et al. 2006. Long-term geological evolution and mass flow balance of the
451 South- Central Andes. In: Oncken, O., Chong, G., Franz, G., Giese, P., Go'tze, H. J., Ramos, V.,
452 Strecker, M. & Wigger, P. (eds) *The Andes – Active Subduction Orogeny*. *Frontiers in Earth*
453 *Sciences*, Springer, Berlin, 1, 401–442.

454 Glodny, J., Echtler, H., Collao, S., Ardiles, M., Burón, P., Figueroa, O., 2008. Differential late
455 paleozoic active margin evolution in South-Central Chile (37° S–40° S)–the Iñalhue fault
456 zone. *Journal of South American Earth Sciences*, 26(4), 397-411.

457 González-Bonorino, F., 1970. Series metamórficas del basamento cristalino de la Cordillera de la
458 Costa de Chile Central. *Departamento de Geología, Universidad de Chile. Publicaciones*, 37, 1–68.

459 González-Bonorino, F., 1971. Metamorphism of the crystalline basement of central Chile. *Journal*
460 *of Petrology*, 12(1), 149-175.

461 González-Bonorino, F., Aguirre, L., 1970. Metamorphic facies series of the crystalline basement of
462 Chile. *Geologische Rundschau*, 59(3), 979-994.

463 Guillaume, B., Moroni, M., Funicello, F., Martinod, J., Faccenna, C., 2010. Mantle flow and
464 dynamic topography associated with slab window opening: Insights from laboratory
465 models. *Tectonophysics*, 496(1-4), 83-98.

466 Hervé, F., Munizaga, F., Godoy, E., Aguirre, L., 1974. Late Paleozoic K/Ar ages of blueschists
467 from Pichilemu, central Chile. *Earth and Planetary Science Letters*, 23(2), 261-264.

468 Hervé, F., 1977. Petrology of the crystalline basement of the Nahuelbuta mountains, southcentral
469 Chile, in: Ishikawa, T., Aguirre L. (Eds). *Comparative studies on the geology of the Circum-Pacific*
470 *Orogenic Belt in Japan and Chile*. Japan Society for the Promotion of Science, Tokyo, pp. 1-51.

471 Hervé, F., Kawashita, K., Munizaga, F. Bassei, M., 1984. Rb–Sr isotopic ages from late Paleozoic
472 metamorphic rocks of Central Chile. *Journal of the Geological Society, London*, 141, 877–884.

473 Hervé, F., 1988. Late Paleozoic subduction and accretion in Southern Chile. *Episodes Journal of*
474 *International Geoscience*, 11(3), 183-188.

475 Hervé, F., Fanning, C.M., Pankhurst, R.J., 2003. Detrital zircon age patterns and provenance in the
476 metamorphic complexes of Southern Chile. *Journal of South American Earth Sciences*, 16, 107–
477 123.

478 Hervé, F., Calderón, M., Fanning, C. M., Pankhurst, R. J., Godoy, E., 2013. Provenance variations
479 in the Late Paleozoic accretionary complex of central Chile as indicated by detrital
480 zircons. *Gondwana Research*, 23(3), 1122-1135.

481 Hyppolito, T., Juliani, C., García-Casco, A., Meira, V. T., Bustamante, A., Hervé, F., 2014a. The
482 nature of the Palaeozoic oceanic basin at the southwestern margin of Gondwana and implications
483 for the origin of the Chilenia terrane (Pichilemu region, central Chile). *International Geology*
484 *Review*, 56(9), 1097-1121.

485 Hyppolito, T., García-Casco, A., Juliani, C., Meira, V. T., Hall, C., 2014b. Late Paleozoic onset of
486 subduction and exhumation at the western margin of Gondwana (Chilenia Terrane):
487 Counterclockwise P–T paths and timing of metamorphism of deep-seated garnet–mica schist and
488 amphibolite of Punta Sirena, Coastal Accretionary Complex, central Chile (34 S). *Lithos*, 206, 409-
489 434.

490 Hyppolito, T., Juliani, C., Garcia-Casco, A., Meira, V., Bustamante, A., Hall, C., 2015. LP/HT
491 metamorphism as a temporal marker of change of deformation style within the Late Palaeozoic
492 accretionary wedge of central Chile. *Journal of Metamorphic Geology*, 33(9), 1003-1024.

493 Kato, T. T., 1985. Pre-Andean orogenesis in the Coast Ranges of central Chile. Geological Society
494 of America Bulletin, 96(7), 918-924.

495 Iwamori, H., 2000. Thermal effects of ridge subduction and its implications for the origin of
496 granitic batholith and paired metamorphic belts. Earth and Planetary Science Letters 181, 131–144.

497 Kato, T.T., Godoy, E., 1995. Petrogenesis and tectonic significance of Late Paleozoic coarse-
498 crystalline blueschist and amphibolite boulders in the coastal range of Chile. International Geology
499 Review, 37, 992–1006

500 Kato, T.T., Sharp, W.D., Godoy, E., 2008. Inception of a Devonian subduction zone along the
501 southwestern Gondwana margin: ^{40}Ar – ^{39}Ar dating of eclogite–amphibolite assemblages in
502 blueschist boulders from the coastal range of Chile (41°S). Canadian Journal of Earth Sciences, 45,
503 337–351.

504 Király, A., Portner, D.E., Haynie, K.L., Chilson-Parks, B.H., Ghosh, T., Jadamec, M., Makushkina,
505 A., Manga, M., Moresi, L., O'Farrel, K.A., 2020. The effect of slab gaps on subduction dynamics
506 and mantle upwelling. Tectonophysics, 785, 228458.

507 Lucassen, F., Trumbull, R., Franz, G., Creixell, C., Vásquez, P., Romer, R. L., Figueroa, O., 2004.
508 Distinguishing crustal recycling and juvenile additions at active continental margins: the Paleozoic
509 to recent compositional evolution of the Chilean Pacific margin (36 – 41°S). Journal of South
510 American Earth Sciences, 17(2), 103-119.

511 Lohrmann, J., 2002. Identification of parameters controlling the accretive and tectonically erosive
512 mass-transfer mode at the South-Central and North Chilean forearc using scaled 2D sandbox
513 experiments, Dissertation, FU Berlin, 2002, Scientific Technical Report STR02/10, [http://www.gfz-
514 potsdam.de/bib/zbstr.htm](http://www.gfz-potsdam.de/bib/zbstr.htm).

515 Marshak, R. S., Karig, D. E., 1977. Triple junctions as a cause for anomalously near-trench igneous
516 activity between the trench and volcanic arc. Geology, 5(4), 233-236.

517 Maruyama, S., Masago, H., Katayama, I., Iwase, Y., Toriumi, M., Omori, S., 2010. A new
518 perspective on metamorphism and metamorphic belts. Gondwana Research, 18(1), 106-137.

519 Martin, M.W., Kato, T.T., Rodriguez, C., Godoy, E., Duhart, P., McDonough, M., Campos,
520 A., 1999. Evolution of the late Paleozoic accretionary complex and overlying forearc-magmatic arc,
521 south central Chile (38° – 41°S): Constraints for the tectonic setting along the southwestern margin of
522 Gondwana. Tectonics, 18, 582-605.

523 Martínez, F., Kania, J., Muñoz, B., Riquelme, R., López, C., 2020. Geometry and development of a
524 hybrid thrust belt in an inner forearc setting: Insights from the Potrerillos Belt in the Central Andes,
525 northern Chile. *Journal of South American Earth Sciences*, 98, 102439.

526 Miyashiro, A., 1961. Evolution of metamorphic belts. *Journal of Petrology*, 2, 277–311.

527 Miyashiro, A., 1972. Metamorphism and related magmatism in plate tectonics. *American Journal of*
528 *Science*, 272, 629-656.

529 Miyashiro, A., 1973. Paired and unpaired metamorphic belts. *Tectonophysics*, 17(3), 241-254.

530 Muñoz-Montecinos, J., Angiboust, S., Cambeses, A., García-Casco, A., 2020. Multiple veining in a
531 paleo-accretionary wedge: The metamorphic rock record of prograde dehydration and transient
532 high pore-fluid pressures along the subduction interface (Western Series, central
533 Chile). *Geosphere*, 16(3), 765-786.

534 Noda, A., 2016. Forearc basins: Types, geometries, and relationships to subduction zone
535 dynamics. *Bulletin*, 128(5-6), 879-895.

536 Nelson, E., Forsythe, R., Diemer, J., Allen, M., and Urbina, O., 1993. Taitao ophiolite: A ridge
537 collision ophiolite in the forearc of southern Chile (46°S). *Revista Geológica de Chile*, 20, 137.

538 Oliveros, V., Vásquez, P., Creixell, C., Lucassen, F., Ducea, M., Ciocca, I., González, J., Espinoza,
539 M., Salazar, E., Coloma, F., Kasemann, S., 2020. Lithospheric evolution of the pre-and early
540 andean convergent margin. *Chile Gondwana Research*, 80, 202–227.

541 Oxburgh, E.R., Turcotte, D.L., 1970. Thermal structure of island arcs. *Geological Society of*
542 *America Bulletin* 81, 1665–1688.

543 Oxburgh, E.R., Turcotte, D.L., 1971. Origin of paired metamorphic belts and crustal dilation in
544 island arc regions. *Journal of Geophysical Research*, 76, 1,315–1,327.

545 Parada, M.A., 1990. Granitoid plutonism in central Chile and its geodynamic implications; a
546 review. *Geological Society of America Special Paper*, 241, 51–66.

547 Parada, M.A., López-Escobar, L., Oliveros, V., Fuentes, F., Morata, D., Calderón, M., Aguirre, L.,
548 Féraud, G., Espinoza, F., Moreno, H., Figueroa, O., Muñoz Ravo, J., Troncoso Vásquez, R., Stern,
549 C.R., 2007. Andean Magmatism. In ‘The Geology of Chile’ (Moreno, T.; Gibson, W.; editors). The
550 Geological Society, London, Special Publication 4: 115-146

551 Pesicek, J. D., Engdahl, E. R., Thurber, C. H., DeShon, H. R. Lange, D., 2012. Mantle subducting
552 slab structure in the region of the 2010 M 8.8 Maule earthquake (30–40 S), Chile. *Geophysical*
553 *Journal International*, 191(1), 317-324.

554 Pineda, G.; Calderón, M., 2008. Geología del área Monte Patria-El Maqui, Región de Coquimbo.
555 Servicio Nacional de Geología y Minería, Carta Geológica de Chile, Serie Geología Básica, 116, 44
556 p., 1 mapa escala 1:100.000.

557 Richter, P., Ring, U., Willner, A. P. Leiss, B. 2007. Structural contacts in subduction complexes and
558 their tectonic significance: the Late Palaeozoic coastal accretionary wedge of central Chile. *Journal*
559 *of the Geological Society*, London, 164, 203–14.

560 Riesner, M., Lacassin, R., Simoes, M., Carrizo, D., Armijo, R., 2018. Revisiting the crustal
561 structure and kinematics of the central Andes at 33.5° S: Implications for the mechanics of Andean
562 Mountain building. *Tectonics*, 37(5), 1347-1375.

563 Roche, V., Sternai, P., Guillou-Frotier, L., Menant, A., Jolivet, L., Bouchot, V., Gerya, T., 2018.
564 Emplacement of metamorphic core complexes and associated geothermal systems controlled by
565 slab dynamics. *Earth and Planetary Science Letters*, 498, 322-333.

566 Rosenbaum, G., Gasparon, M., Lucente, F.P., Peccerillo, A., Miller, M.S., 2008. Kine-matics of
567 slab tear faults during subduction segmentation and implications for Italian magmatism. *Tectonics*,
568 27.

569 Santosh, M., Kusky, T., 2010. Origin of paired high pressure–ultrahigh-temperature orogens: a
570 ridge subduction and slab window model. *Terra Nova*, 22(1), 35-42.

571 Schubert, G., Yuen, D. A., and Turcotte, D. L., 1975. Role of phase transitions in a dynamic mantle.
572 *Geophysical Journal of the Royal Astronomical Society*, 42, 705–735.

573 Shibata, K., Ishihara, S., Ulriksen, C., 1984. Rb-Sr ages and initial $^{87}\text{Sr}/^{86}\text{Sr}$ ratios of late Paleozoic
574 granitic rocks from northern Chile. *Bulletin of the Geological Survey of Japan*, 35 (2), 537-545.

575 Sigoña León, P. A., 2016. Petrología, geocronología e implicancias tectónicas de enclaves
576 graníticos del paleozoico tardío en un dique mesozoico en el sector costero del Norte Chico (31
577 30'S), Chile.

578 Sisson, V. B., Pavlis, T. L., Roeske, S. M., Thorkelson, D. J., 2003. Introduction: An overview of
579 ridge-trench interactions in modern and ancient settings. *Geological Society of America Special*
580 *Paper*, 371, 1-18.

581 Stern, R. J., 2002. Subduction zones. *Reviews of geophysics*, 40(4), 3-1.

582 Tatsumi, Y., 2005. The subduction factory: How it operates in the evolving Earth. *GSA Today* 15,
583 4–10.

584 Thorkelson, D. J., Madsen, J. K., Slaggett, C. L., 2011. Mantle flow through the Northern
585 Cordilleran slab window revealed by volcanic geochemistry. *Geology*, 39(3), 267-270.

586 Underwood, M.B., Byrne, T., Hibbard, J.P., DiTullio, L., Laughland, M.M., 1993. The effects of
587 ridge subduction on the thermal structure of accretionary prisms: a Tertiary example from the
588 Shimanto Belt of Japan. In: Underwood, M.B. (Ed.), *Thermal Evolution of the Tertiary Shimanto*
589 *Belt, Southwest Japan: An Example of Ridge –trench Interaction*. Special Paper, vol. 273.
590 Geological Society of America, Boulder, Colorado, pp. 151 – 168.

591 Uyeda, S., Miyashiro, A., 1974. Plate tectonics and the Japanese Islands: a synthesis. *Geological*
592 *Society of America Bulletin*, 85(7), 1159-1170.

593 Uyeda, S., Kanamori, H., 1979. Back-arc opening and the mode of subduction. *Journal of Geo-*
594 *physical Research, Solid Earth*, 84, 1049–1061.

595 Wakabayashi, J., 2004. Tectonic mechanisms associated with P–T paths of regional metamorphism:
596 alternatives to single-cycle thrusting and heating. *Tectonophysics*, 392(1-4), 193-218.

597 Willner, A.P., Hervé, F., Massonne, H.J., 2000. Mineral chemistry and pressure-temperature
598 evolution of two contrasting high-pressure-low-temperature belts in the Chonos archipelago,
599 Southern Chile. *Journal of Petrology*, 41, 309-330.

600 Willner, A. P., Glodny, J., Gerya, T. V., Godoy, E., Massonne, H. J., 2004. A counterclockwise PTt
601 path of high-pressure/low-temperature rocks from the Coastal Cordillera accretionary complex of
602 south-central Chile: constraints for the earliest stage of subduction mass flow. *Lithos*, 75(3-4), 283-
603 310.

604 Willner, A. P., 2005. Pressure–temperature evolution of a Late Palaeozoic paired metamorphic belt
605 in North–Central Chile (34°–35° 30' S). *Journal of Petrology*, 46(9), 1805-1833.

606 Willner, A. P., Thomson, S. N., Kröner, A., Wartho, J. A., Wijbrans, J. R., Hervé, F., 2005. Time
607 markers for the evolution and exhumation history of a Late Palaeozoic paired metamorphic belt in
608 North–Central Chile (34°–35° 30' S). *Journal of Petrology*, 46(9), 1835-1858.

609 Willner, A. P., Gerdes, A., Massonne, H. J., 2008. History of crustal growth and recycling at the
610 Pacific convergent margin of South America at latitudes 29–36 S revealed by a U–Pb and Lu–Hf

611 isotope study of detrital zircon from late Paleozoic accretionary systems. *Chemical Geology*, 253(3-
612 4), 114-129.

613 Willner, A. P., Richter, P. P., Ring, U., 2009. Structural overprint of a late Paleozoic accretionary
614 system in north-central Chile (34-35°S) during post-accretional deformation. *Andean*
615 *Geology*, 36(1), 17-36.

616 Willner, A. P., Gerdes, A., Massonne, H. J., Schmidt, A., Sudo, M., Thomson, S. N., Vujovich, G.,
617 2011. The geodynamics of collision of a microplate (Chilenia) in Devonian times deduced by the
618 pressure–temperature–time evolution within part of a collisional belt (Guarguaraz Complex, W-
619 Argentina). *Contributions to Mineralogy and Petrology*, 162(2), 303-327.

620 Wortel, M. J. R., Spakman, W., 2000. Subduction and slab detachment in the Mediterranean-
621 Carpathian region. *Science*. 290(5498), 1910-1917.